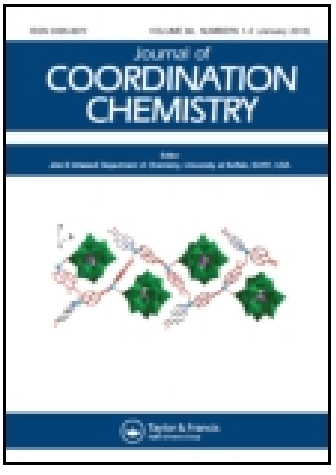

Journal of Coordination Chemistry
Publication details, including instructions for authors and subscription information:
http://www.tandfonline.com/loi/gcoo20

Dinuclear phenoxo-bridged "end-off" complexes containing a piperazine that shows chemical nuclease and cytotoxic activities

C. Karthick[a], P. Gurumoorthy[a], M.A. Imran Musthafa[a], Rachita Lakra[b], Purna Sai Korrapati[b] & A. Kalilur Rahiman[a]

[a] Post-Graduate and Research Department of Chemistry, The New College (Autonomous), Chennai, India

[b] Biomaterials Division, CSIR-Central Leather Research Institute, Chennai, India

Accepted author version posted online: 06 May 2014.Published online: 02 Jun 2014.

To cite this article: C. Karthick, P. Gurumoorthy, M.A. Imran Musthafa, Rachita Lakra, Purna Sai Korrapati & A. Kalilur Rahiman (2014) Dinuclear phenoxo-bridged "end-off" complexes containing a piperazine that shows chemical nuclease and cytotoxic activities, Journal of Coordination Chemistry, 67:10, 1794-1808, DOI: 10.1080/00958972.2014.920501

To link to this article: http://dx.doi.org/10.1080/00958972.2014.920501

Journal of Coordination Chemistry, 2014
Vol. 67, No. 10, 1794–1808, http://dx.doi.org/10.1080/00958972.2014.920501

Dinuclear phenoxo-bridged "end-off" complexes containing a piperazine that shows chemical nuclease and cytotoxic activities

C. KARTHICK†, P. GURUMOORTHY†, M.A. IMRAN MUSTHAFA†, RACHITA LAKRA‡, PURNA SAI KORRAPATI‡ and A. KALILUR RAHIMAN*†

†Post-Graduate and Research Department of Chemistry, The New College (Autonomous), Chennai, India
‡Biomaterials Division, CSIR-Central Leather Research Institute, Chennai, India

(*Received 10 July 2013; accepted 20 March 2014*)

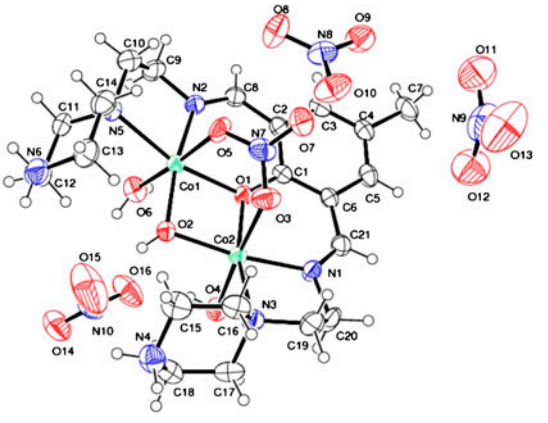

Three dinuclear cobalt(II), nickel(II), and copper(II) complexes (**1–3**) of a phenol-based 'end-off' compartmental ligand, 2,6-bis[1-(N-ethyl)piperazineiminomethyl]-4-methylphenol (HL), have been synthesized and characterized by spectral analysis. The molecular structure of one of these complexes, 2,6-bis[1-(N-ethyl)piperazineiminomethyl]-4-methylphenolato-diaqua-μ-hydroxo-μ-nitrato-dicobalt(II) nitrate, $[Co_2(H_2L)(\mu\text{-}OH)(\mu\text{-}NO_3)(H_2O)_2](NO_3)_3]$ (**1**), was determined by single crystal X-ray crystallography. The complex exhibits a distorted octahedral geometry around cobalt with a Co–Co distance of 2.9882(8) Å. Electrochemical studies of **1–3** reveal that the redox processes are due to ligand reactions. The EPR spectrum of **3** showed a broad signal at $g = 2.11$ indicating magnetic interaction between the two copper ions. The μ_{eff} values for **1** and **3** are 4.94 and 1.93 BM, respectively, which indicate a spin–spin interaction between the metal ions. Complex **3** caused a cleavage of circular plasmid pBR322 DNA into nicked circular and linear forms in the presence of a co-reactant. Human epidermoid carcinoma cells, A431, were employed for *in vitro* cytotoxicity studies of the synthesized complexes. The IC_{50} value of **3** is lower than that of the other two complexes. The copper complex (**3**) exhibited better chemical nuclease and cytotoxic activity than the other two complexes.

*Corresponding author. Emails: newcollege87@gmail.com; akrahmanjkr@gmail.com

Keywords: Dinuclear complexes; Crystal structure; Cyclic voltammetry; Chemical nuclease activity; Cytotoxicity

1. Introduction

Attention has been devoted to develop effective, less toxic, and site-specific metal-based anticancer drugs [1]. DNA is the primary target of such drugs since it possesses suitable metal-binding sites in its structure. The success of platinum-based complexes as anticancer agents forms the basis for involving transition metal complexes as small molecules for targeting cancer cells [2]. The interaction of such small molecules with the DNA of cancer cells affects the cell division and hence, ceases further growth of cancer cells [3]. Transition metal complexes offer diversified features such as structures, redox, and physicochemical properties which make them suitable for applications including medicine and biotechnology [4].

Compartmental ligands, comprised of macrocyclic and acyclic systems having two or more coordination chambers in close proximity, provide selective recognition of charged and/or neutral species at their adjacent chambers. Acyclic compartmental ligands have been classified as "end-off," "side-off," and polypodal ligands. "End-off" complexes are provided with one endogenous and one exogenous bridge "side-off" complexes, with two endogenous bridges, whereas the polypodal complexes are provided with two bridges among which, one is endogenous and the other exogenous bridge may be offered by a suitable anion. Acyclic multinucleating ligands possessing two chelating arms and central donor bridges are called "end-off" compartmental ligands. The complexes of these ligands have different bridging features, which creates an interest in coordination chemistry [5, 6].

"End-off" compartmental dinuclear complexes have been studied for biological significance such as urease active site, catechol oxidase, biosites like hemerithryne, ribonucleotide reductase, phospholipase C, phosphotases, and aminopeptidases; antimicrobial, antiproliferative, and superoxide dismutase activities [7–14]. Phenol-based "end-off" compartmental ligands possessing piperazine chelating arms have been rarely used for bimetallic biosites [15–18]. Understanding the mechanism of DNA cleavage by small molecules along with the role of active species involved can be correlated to the cytotoxicity of small molecules [19]. Herein, we report the synthesis, spectral, magnetic, and electrochemical properties of dinuclear cobalt(II), nickel(II), and copper(II) complexes derived from an "end-off" compartmental ligand containing a piperazine side arm, 2,6-bis[1-(N-ethyl)piperazineiminomethyl]-4-methylphenol (HL). The chemical nuclease and cytotoxic activities were performed to test their biological efficacy.

2. Experimental set-up

2.1. *Materials and methods*

2,6-Diformyl-4-methylphenol has been synthesized according to the literature method [20, 21]. N-(2-aminoethyl)piperazine was purchased from Sigma-Aldrich Ltd., USA. 4-Methylphenol and hexahydrates of metal(II) nitrates were purchased from Sd-fine chemicals (India), and the supercoiled (SC) pBR322 DNA was obtained from Genei (India). Solvents were purified by adapting reported procedures [22]. Tetra(*n*-butyl)ammonium perchlorate (TBAP) used as the supporting electrolyte in the electrochemical measurements was purchased from Fluka and recrystallized from hot methanol. All other chemicals and

solvents were purchased from commercial sources and used without purification. Microanalyses (% C, H, and N) were performed using a Carlo Erba model 1106 Elemental analyzer. Infrared spectra were recorded on an ABB Instruments, MB-3000 spectrophotometer using KBr pellets from 4000 to 400 cm^{-1}. ^{1}H and ^{13}C NMR spectral data were collected on a Varian-VNMRS-400 in $CDCl_3$ solution with tetramethylsilane as an internal standard at ambient temperature. EI mass spectrum of ligand was recorded using JEOL GCMATE II GC-MS and ESI mass spectra of complexes were recorded using a Q-Tof Mass spectrometer. Electronic spectra were recorded using a Perkin Elmer Lambda-45 spectrophotometer from 200 to 1100 nm. X-band EPR spectra were recorded on a Varian EPR-E 112 spectrometer using diphenylpicrylhydrazine as the reference. Variable-temperature magnetic susceptibilities were recorded in a Lake Shore Cryotronics Inc., Vibrating Sample Magnetometer Model 7410. Cyclic voltammograms were recorded on an electrochemical workstation of CH instruments (602D) in an oxygen-free atmosphere using TBAP as the supporting electrolyte (*Caution*: TBAP is potentially explosive and hence, care must be taken while handling this compound).

2.2. *Synthesis of 2,6-bis[1-(N-ethyl)piperazineiminomethyl]-4-methylphenol (HL)*

To a 50 mL methanolic solution of 2,6-diformyl-4-methylphenol (1.64 g, 10 mM), N-(2-aminoethyl)piperazine (2.62 mL, 20 mM) was added dropwise with constant stirring, and the mixture was refluxed for 6 h while the color changes from yellow to orange–red. The red oil-type compound was obtained on slow evaporation of the solvent. The product was washed with diethyl ether followed by cold methanol and dried in vacuum.

Yield: 1.91 g (49%). Anal. Calcd for $C_{21}H_{34}N_6O$ (%): C, 65.24; H, 8.86; N, 21.74. Found (%): C, 65.22; H, 8.95; N, 21.76. Selected IR data (KBr disk, ν cm^{-1}): 3420 ν(OH), 2950 ν(N–H), 1644 ν(C=N). EI-MS: (*m/z*) 387.09. ^{1}H NMR ($CDCl_3$, 400 MHz) δ: 2.51 (s, 3H, CH_3), 2.29–2.91 (m, 16H, CH_2), 3.74–3.78 (m, 8H, CH_2) 5.45 (br s, 2H, NH), 7.45 (s, 2H, Ar–H), 8.55 (s, 2H, CH=N), 10.23 (s, H, OH). ^{13}C NMR ($CDCl_3$, 100.50 MHz) δ: 20.22 (CH_3), 45.98 (2 CH_2), 54.62–59.42 (4 CH_2), 127.45 (Ar C), 159.27 (C–OH), 165.23 (C=N).

2.3. *Preparation of dinuclear complexes*

2.3.1. 2,6-Bis[1-(N-ethyl)piperazineiminomethyl]-4-methylphenolato-diaqua-μ-hydroxo-μ-nitrato-dicobalt(II) nitrate (1). To a methanolic solution (25 mL) of HL (0.39 g, 1 mM), $Co(NO_3)_2{\cdot}6H_2O$ (0.73 g, 2.5 mM) in methanol (25 mL) was added dropwise with constant stirring and then refluxed for 3 h. The solvent was evaporated to one-third of the original volume, filtered, and kept in a $CaCl_2$ desiccator. Dark brown crystals of the complex suitable for X-ray diffraction studies were obtained.

Yield: 0.59 g (73%). Anal. Calcd for $C_{21}H_{40}N_{10}O_6Co_2$ (%): C, 31.28; H, 4.99; N, 17.36. Found (%): C, 31.26; H, 5.05; N, 17.37. Selected IR data (KBr disk, ν cm^{-1}): 3380 ν(OH), 1633 ν(C=N), 1600 ν(NH_2). UV–vis [H_2O, λ_{max} (nm) ($\varepsilon/M^{-1}\,cm^{-1}$)]: 560 (100), 394 (4608), 263 (16,250). ESI-MS in methanol (*m/z*): 728.07 $[Co_2L + H_2O + OH + 3NO_3 + 2H]^+$, 627.07 $[Co_2L + 2NO_3]^+$.

2.3.2. 2,6-Bis[1-(N-ethyl)piperazineiminomethyl]-4-methylphenolato-diaqua-μ-hydroxo-μ-nitrato-dinickel(II) nitrate (2). This complex was synthesized from HL (0.39 g, 1 mM)

and $Ni(NO_3)_2{\cdot}6H_2O$ (0.73 g, 2.5 mM) by following the procedure reported for **1**. A pale green precipitate obtained was washed with diethyl ether and dried under vacuum.

Yield: 0.56 g (69%). Anal. Calcd for $C_{21}H_{40}N_{10}O_6Ni_2$ (%): C, 31.29; H, 5.00; N, 17.37. Found (%): C, 31.26; H, 5.08; N, 17.39. Selected IR data (KBr disk, ν cm^{-1}): 3375 ν(OH), 1628 ν(C=N), 1567 $\nu(NH_2)$. UV–vis [H_2O, λ_{max} (nm) ($\varepsilon/M^{-1}\,cm^{-1}$)]: 954 (300), 587 (860), 400 (1000), 274 (15,630). ESI-MS in methanol (*m/z*): 645.95 $[Ni_2L + 2NO_3 + OH + H]^+$, 503.92 $[Ni_2L]^+$.

2.3.3. 2,6-Bis[1-(N-ethyl)piperazineiminomethyl]-4-methylphenolato-diaqua-μ-hydroxo-μ-nitrato-dicopper(II) nitrate (3). This complex was synthesized from HL (0.39 g, 1 mM) and $Cu(NO_3)_2{\cdot}6H_2O$ (0.60 g, 2.5 mM) by following the procedure reported for **1**. A dark green precipitate obtained was washed with diethyl ether and dried under vacuum.

Yield: 0.53 g (65%). Anal. Calcd for $C_{21}H_{40}N_{10}O_6Cu_2$ (%): C, 30.92; H, 4.94; N, 17.17. Found (%): C, 30.89; H, 5.03; N, 17.19. Selected IR data (KBr disk, ν cm^{-1}): 3367 ν(OH), 1620 ν(C=N), 1544 $\nu(NH_2)$. UV–vis [H_2O, λ_{max} (nm) ($\varepsilon/M^{-1}\,cm^{-1}$)]: 648 (100), 372 (2100), 292 (4700). ESI-MS in methanol (*m/z*): 691.69 $[Cu_2L + 2H_2O + OH + 2NO_3 + H]^+$, 575.65 $[Cu_2L + NO_3]^+$.

2.4. *X-ray crystallographic studies*

Crystals of **1** were sorted using a polarizing microscope (Leica DMLSP). Crystals were cut to suitable size and mounted on a Kappa Apex2 CCD diffractometer equipped with graphite monochromated Mo(Kα) radiation ($\lambda = 0.71073$ Å). The intensity data were collected using ω and φ scans with a frame width of 1°. The frame integration and data reduction were performed using Bruker SAINT-plus (Version 7.06a) software [23]. Multiscan absorption corrections were applied to the data using SADABS [24]. The sample was stable at room temperature. The structure was solved using SIR92 [25]. Full-matrix least-squares refinement was performed using SHELXL-97 (Sheldrick, 1997).

2.5. *Chemical nuclease activity*

The cleavage of SC pBR322 DNA was monitored using the agarose gel electrophoresis technique in which SC DNA (33.3 μM) was treated with the synthesized "end-off" complexes (**1–3**) in 5 mM Tris[tris(hydroxymethyl)aminomethane]–HCl/50 mM NaCl buffer (pH 7.2) in the absence and the presence of the co-reactant. In each experiment, 4 μL of plasmid DNA was treated with 6 μL metal complexes of concentrations 50, 100, and 200 μM along with H_2O_2 as a co-reactant (2 μL, 40 μM), and the samples were incubated for 1.5 h at 37 °C. A loading buffer containing 0.25% bromophenol blue, 0.25% xylene cyanol, and 30% glycerol (3 μL) was added, and the electrophoresis of the DNA was performed on agarose gel (0.8%) stained with ethidium bromide (1 μg/mL). The gels were run at 50 V for 1 h in TAE buffer (40 mM Tris base, 20 mM acetic acid, 1 mM EDTA, pH 8.3). The resulting bands were visualized by UV light and photographed.

2.6. *Cytotoxic activity*

The effect of **1–3** on human epidermoid carcinoma cell lines (A431) was evaluated by performing MTT (3-(4,5-dimethylthiazol-2-yl)-2,5-diphenyltetrazolium bromide) assay [26].

Cells were seeded in 48 well plates (8000 cells/well) containing Dulbecco's modified eagle medium (DMEM) with 10% Fetal Bovine Serum (FBS), allowed to adhere, and maintained for 24 h. Later, the medium was replaced with DMEM containing 1% serum. The 12.5, 25, 125, 250, and 500 μM concentrations of complexes were dissolved in water and added to the cells. The test samples were kept in triplicate. Controls were maintained under similar conditions without the influence of compounds under study. The plate was incubated at 37 °C in 5% CO_2. After 24 h, MTT stock solution (5 mg/mL) was added to each culture well, equal to one-tenth of the original culture volume and incubated at 37 °C for 3–4 h. At the end of the incubation period, the medium was removed and the blue–purple formazan crystals formed were solubilized with DMSO. Later, the cell viability was measured spectrophotometrically at 570 nm using a multi-plate reader, and the percentage of cell viability was evaluated using the following equation:

$$\text{Cell viability}\,(\%) = [A_{570}(\text{sample})/A_{570}(\text{control})] \times 100$$

where A_{570}(sample) refers to the reading from the wells treated with the complexes, and A_{570}(control) refers to that from the wells treated with the medium containing 10% FBS only.

3. Results and discussion

The "end-off" compartmental ligand, HL, was synthesized by treating one equivalent of 2,6-diformyl-4-methylphenol with two equivalents of N-(2-aminoethyl)piperazine, and characterized by regular physico-chemical techniques. Complexes **1–3** were prepared by the reaction of HL with the corresponding metal(II) nitrates (1 : 2.5) in methanol (scheme 1) and characterized by microanalysis, IR, UV–vis, and mass spectroscopy. Electrochemical, magnetic, chemical nuclease, and cytotoxic studies were also carried out for all the complexes.

3.1. *Crystal structure*

The molecular structure along with atom labeling of **1**, $[Co_2(H_2L)(\mu\text{-}OH)(\mu\text{-}NO_3)(H_2O)_2](NO_3)_3$ is given in figure 1. Crystal data and structure refinement are given in table 1 while selected bond lengths and angles are summarized in table 2. Single crystal diffraction analysis reveals that **1** crystallizes as trigonal crystal system with space group *p65*. The constitution of the deprotonated Schiff base ligand (HL) is as expected with the phenolate group acting as an endogenous bridge. This bridge is markedly symmetric with Co(1)–O(1) and Co(2)–O(1) distances of 2.078(3) and 2.080(2) Å, respectively. In addition, there are two exogenous bridges: a hydroxyl and a nitrate. The hydroxyl bridge is symmetric with Co(1)–O(2) and Co(2)–O(2) distances of 1.991(3) and 1.980(3) Å, respectively. The nitrate is also bound symmetrically with Co(1)–O(5) and Co(2)–O(3) at 2.167(3) and 2.239(4) Å, respectively. Two water molecules are coordinated to Co(1) and Co(2) through O(6) and O(4), respectively, with similar Co–O distances of 2.179(3) and 2.187(3) Å with respect to Co(1)–O(6) and Co(2)–O(4).

Each cobalt ion is six-coordinate, and the donor sets are completed by two nitrogens from the side arms. The two Co–N (metal-imine nitrogen) distances viz., Co(1)–N(2) 2.045(3) Å and Co(2)–N(1) 2.035(4) Å are identical. The geometry around each of the two

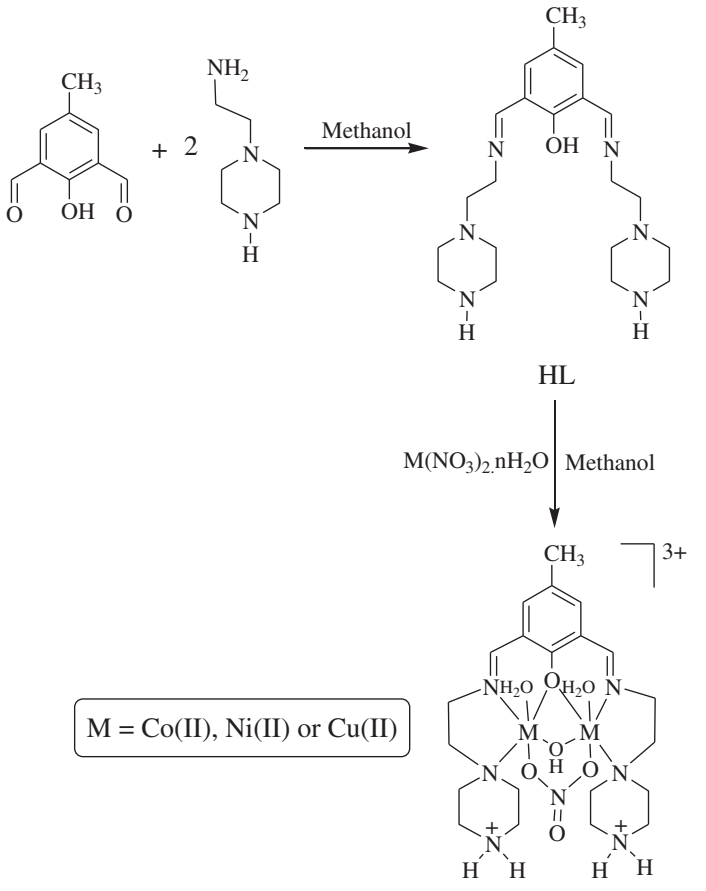

Scheme 1. Synthetic route for the phenoxo-bridged dinuclear "end-off" complexes.

cobalt(II) nuclei is best described as distorted octahedral, formed by coordination of each cobalt(II) with a phenolate oxygen, an imine nitrogen, a piperazine nitrogen, one water molecule, and two bridges formed by hydroxyl and nitrate groups. The Co(1)–Co(2) distance is 2.9882(8) Å which is typical for binuclear Co(II) complexes [27]. As expected, the piperazine rings adopt the chair conformation and protonation of the uncoordinated amine nitrogens of piperazine moieties that balance the charge of the complex with the presence of three uncoordinated nitrates.

3.2. *Spectral characterization*

The IR spectrum of the ligand showed a broad band at 3420 cm^{-1} due to the presence of the phenolic ν(OH), and the broadness is due to intermolecular hydrogen bonding between the phenolic and azomethine groups. A medium intensity band at 2950 cm^{-1} is attributed to ν(N–H). The sharp band at 1644 cm^{-1} corresponds to the –C=N stretch and, on complexation, shifts to lower frequency (1633–1620 cm^{-1}), indicating binding of the metal ion to nitrogen of azomethine. A band observed at 1600–1544 cm^{-1} for **1–3** may be assigned to

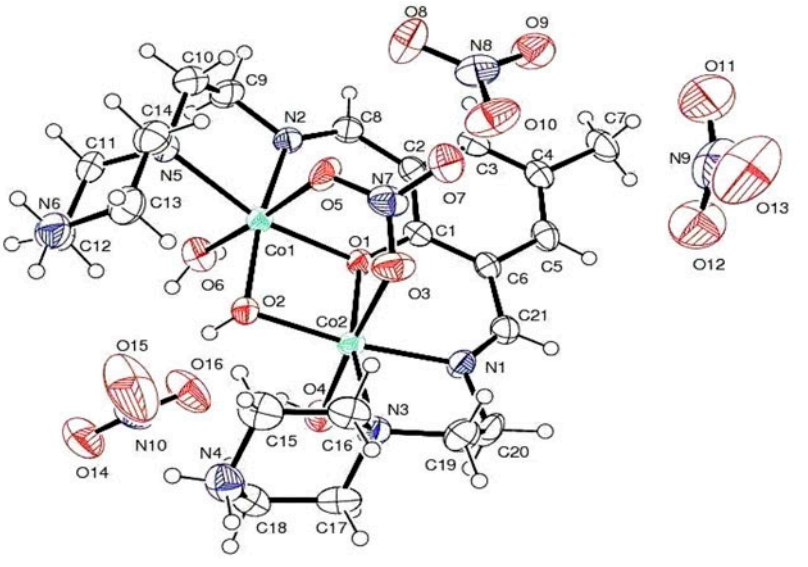

Figure 1. ORTEP diagram of **1** showing an atom-labeling scheme. Displacement ellipsoids are drawn at the 30% probability level.

Table 1. Crystal data and structure refinement for **1**.

Empirical formula	$C_{21}H_{40}N_{10}O_{16}Co_2$
Formula weight	806.49
Temperature	293 ± 2 K
Wavelength	0.71073 Å
Crystal system	Trigonal
Space group	*p65*
Unit cell dimensions	
a (Å)	9.95400(10)
b (Å)	9.95400(10)
c (Å)	57.5400(8)
α (°)	90
β (°)	90
γ (°)	120
Volume (Å^3)	4937.37(10)
Z	6
Calculated density (Mg m^{-3})	1.627
Adsorption coefficient (mm^{-1})	1.094
F (0 0 0)	2508
Crystal size (mm)	0.20 × 0.20 × 0.15
Index ranges	$-7 \le h \le 11$, $-11 \le k \le 7$, $-58 \le l \le 38$
Reflections collected	12,458
Independent reflections	4137 [R(int) = 0.0242]
Refinement method	Full-matrix least-squares on F^2
Data/restraints/parameters	4137/14/490
GOF on F^2	1.032
Final R indices [$I < 2\sigma(I)$]	$R_1 = 0.0296$, $wR_2 = 0.0604$
R indexes (all data)	$R_1 = 0.0347$, $wR_2 = 0.0627$
Largest diff. peak and hole	0.284 and –0.232 e Å^{-3}

Table 2. Selected bond lengths (Å) and angles (°) for **1**.

Bond lengths (Å)			
Co(1)–O(1)	2.078(3)	Co(2)–O(2)	1.980(3)
Co(1)–O(2)	1.991(3)	Co(2)–O(3)	2.239(3)
Co(1)–O(5)	2.167(3)	Co(2)–O(4)	2.187(3)
Co(1)–O(6)	2.179(3)	Co(2)–N(1)	2.035(4)
Co(1)–N(2)	2.045(3)	Co(2)–N(3)	2.256(3)
Co(1)–N(5)	2.257(4)	Co(1)–Co(2)	2.9882(8)
Co(2)–O(1)	2.080(2)		
Bond angles (º)			
Co(1)–O(1)–Co(2)	91.89(10)	N(2)–Co(1)–Co(2)	129.51(11)
Co(2)–O(2)–Co(1)	97.60(12)	N(1)–Co(2)–Co(1)	129.04(9)
N(2)–Co(1)–O(1)	86.02(12)	N(3)–Co(2)–Co(1)	144.21(10)
N(5)–Co(1)–Co(2)	145.31(9)	N(1)–Co(2)–O(4)	87.28(14)
N(2)–Co(1)–O(6)	85.58(14)	N(1)–Co(2)–O(3)	89.05(13)
N(2)–Co(1)–O(5)	89.29(13)	N(1)–Co(2)–N(3)	82.00(14)
O(6)–Co(1)–N(5)	92.69(14)	O(3)–Co(2)–N(3)	86.77(12)
N(2)–Co(1)–N(5)	81.97(13)	O(4)–Co(2)–N(3)	93.08(12)
O(5)–Co(1)–N(5)	85.56(13)	O(2)–Co(1)–O(5)	93.88(12)
O(1)–Co(1)–N(5)	165.35(11)	O(2)–Co(1)–O(6)	91.35(13)
N(1)–Co(2)–O(1)	86.27(12)	O(2)–Co(2)–O(4)	93.48(14)
O(1)–Co(2)–N(3)	165.52(13)	O(2)–Co(2)–O(3)	90.07(13)

$\nu(NH_2)$, which suggests protonation of the terminal nitrogen of the amine. Broad bands for the complexes at 3380–3367 and 513–547 cm^{-1} are assigned to the ν(OH) of coordinated water and ν(M–O), respectively. The intense bands at 1540–1530 cm^{-1} can be assigned to bridging phenoxide [28]. Bands at 1344–1308 and 1046–1032 cm^{-1} suggest the presence of coordinated nitrate, whereas the band at 1396–1352 cm^{-1} is attributable for ionic nitrate [29, 30].

Electronic spectra of **1–3** are recorded in water and exhibit the following salient features. The intense peak below 300 nm is assigned to an intra-ligand charge transfer transition. The medium intensity broad band at 372–400 nm is ascribed to ligand-to-metal charge transfer transitions [31]. The d–d transition for **1** obtained at 560 nm falls within the range for an octahedral complex. Complex **2** exhibits bands at 587 and 954 nm which are well suited for a distorted octahedral geometry. Absorption spectrum of **3** reveals its octahedral geometry like other Cu(II) complexes [32] by exhibiting a band at 648 nm. The solid-state ESR spectrum of **1** is recorded at liquid nitrogen temperature and for **3** at room temperature. Complex **3** exhibits a broad spectrum (figure 2) with no hyperfine splitting with a value for $g = 2.11$, indicating the presence of antiferromagnetic interaction between copper ions [33, 34]. The g value for **1** is 3.04 and the large deviation in g value from the spin-only value ($g = 2.0023$) is due to a large angular momentum contribution.

3.3. *Magnetochemistry*

The observed room temperature magnetic moment (μ_{eff}) values for the dinuclear "end-off" complexes **1** and **3** are 4.94 and 1.93 BM, respectively, which lie in the range reported for six-coordinate Co(II) and Cu(II) complexes [35, 36], conveying the presence of antiferromagnetic interaction between the two metal(II) ions. Temperature-dependent magnetic susceptibility data for **3** were obtained to gain information about magnetic exchange interactions. The magnetic susceptibility data for dry, powdered sample were measured from

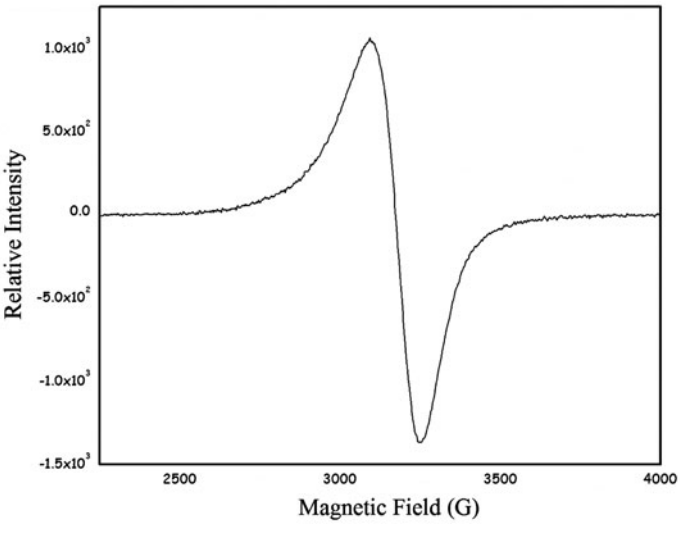

Figure 2. X-band EPR spectrum of **3**.

20 to 300 K using a variable magnetometer using an applied external magnetic field of 0.2 T. The plots of χ_M and $\chi_M T$ *versus* T are depicted in figure 3. The observed χ_M value at 300 K is 0.204×10^{-3} cm^3 M^{-1}, which gradually increases on lowering the temperature from 300 to 50 K and then suddenly increases to 1.5×10^{-3} cm^3 M^{-1} at 20 K. Usually in dinuclear complexes the change in magnetic moment with temperature is supported by three factors: contribution of the orbital momentum, intramolecular magnetic coupling between two

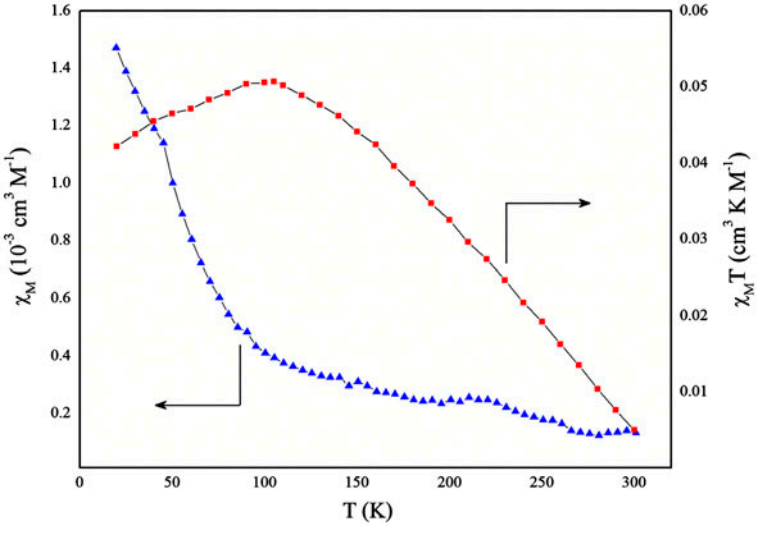

Figure 3. Plots showing the temperature dependence of χ_M and $\chi_M T$ for **3**.

metal ions, and intermolecular antiferromagnetic coupling [37]. The antiferromagnetic coupling between the two Cu ions through the bridging phenoxide ion is attributed to the unusual magnetic behavior of the complex [38]. This is complemented by a broad EPR spectrum with no hyperfine splitting. The $\chi_M T$ *versus* T plot is also indicative of strong antiferromagnetic coupling exchange interaction between adjacent copper ions. The value starts increasing from $0.005\,cm^3\,K\,M^{-1}$ at 300 K, with lowering the temperature reaching a maximum at 100 K, and it decreases to $0.042\,cm^3\,K\,M^{-1}$ at 20 K. The singlet–triplet energy separation ($-2J$) is evaluated by fitting the magnetic susceptibility values to the modified Bleany–Bowers equation [39].

$$\chi_M = (Ng^2\beta^2/3kT)[3 + \exp(-2J/kT)]^{-1}(1 - P) + (0.45P/T) + N_\alpha$$

where χ_M is the paramagnetic susceptibility per metal atom, N is the Avogadro's number, g is the average gyromagnetic ratio, N_α is the temperature-independent fraction usually assumed to be $120 \times 10^{-6}\,cm^3\,M^{-1}$ for Cu(II) compounds, β is the Bohr magneton, k is the Boltzmann's constant, and P is the fraction of paramagnetic monomeric copper(II) impurities. The exchange integral ($-2J$) value observed for **3** is $209\,cm^{-1}$. The exchange interactions are primarily controlled by the Cu–O–Cu bridge angle. In addition to that, it is also influenced by the electronegativity of the bridging atom, degree of distortion from planar geometry, and dihedral angle between two copper planes [40].

3.4. *Electrochemistry*

In general, "end-off" complexes show quasi-reversible or irreversible waves in the cathodic potential region [41, 42]. The electrochemical behaviors of ligand (HL) and **1–3** have been studied by cyclic voltammetry in DMF containing 0.1 M TBAP (table S1 and figures S1 and S2, Supplementary material, see online at http://dx.doi.org/10.1080/00958972.2014.920501). The nature of reduction and oxidation waves obtained for the complexes resembles the ones obtained for HL. The complexes exhibit two irreversible waves in the cathodic as well as anodic regions, and a one-electron transfer can be assumed for each wave. The reduction potential values E^1_{pc} and E^2_{pc} are in the range –0.71 to –0.73 V and –1.38 to –1.48 V, respectively, whereas the oxidation potential values E^1_{pa} and E^2_{pa} are 0.58–0.94 V and 0.88–1.53 V, respectively. In the anodic region, **3** exhibits two peaks around 0.60 and 0.94 V, and usually the oxidation of Cu(II) is not feasible [43]. Thus, the observed peaks are attributed to ligand reactions [44]. Based on these facts, we can conclude that the redox processes of **1–3** are due to ligand reactions and the metal ions have no influence on their redox behavior.

3.5. *Chemical nuclease activity*

DNA cleavage chemistry associated with redox-active or photo-activated metal complexes is a useful tool in the characterization of DNA recognition of transition metal complexes [45]. Different DNA cleavage efficiencies of complexes may occur due to different binding affinities of complexes to the DNA [46]. In the gel electrophoresis method, segregation of molecules is based on the relative rate of movement over the gel under the influence of the electric field. DNA is negatively charged and when it is placed in an electric field, it will migrate towards the anode and the extent of migration of DNA depends on the strength of the electric field, nature of buffer, density of agarose gel, and DNA size. DNA cleavage is

controlled by relaxation of the SC circular form of pBR322 into the nicked circular (NC) and linear circular (LC) forms. When circular plasmid DNA is run on horizontal gel using electrophoresis, the fastest migration will be observed for the SC form (Form I). NC form (Form II) will be produced as a consequence of relaxation of the SC form, when a single strand of DNA alone is cleaved. On the other hand, a LC (Form III) that migrates in between Form II and Form I will be generated when both strands of DNA are cleaved [47].

Figure 4(a)–(c) represents the cleavage of SC DNA in the presence of **1–3** of concentrations 50, 100, and 200 μM. However, for **1**, appreciable cleavage is not obtained in this concentration range, but at lower concentrations such as 6.25, 12.5, and 25 μM cleavage is observed. The cleavage efficacy of all complexes increases with increasing concentration of the complexes.

3.5.1. Nuclease activity in the absence of co-reactant. Hydrolytic cleavage is a simple form of nuclease activity which does not require any external agents. Lanes 2, 4, and 6 [figure 4(a)–(c)] represent the nuclease activity of **1–3** in the absence of co-reactant. From these lanes, it is evident that there is a decrease in intensity of Form I (SC) with increase in intensity of Form II (NC) without any evidence of Form III (LC), indicating a single-strand DNA breaking by all the complexes. A plausible mechanism for the hydrolytic cleavage promoted by the dinuclear(II) complexes, based on reports from the literature [48, 49], is depicted in scheme 2. Here, the cleavage may be activated by nucleophilic attack on the phosphodiester bonds via charge neutralization by the Lewis acidity of the central metal ion. Moreover, the water molecules associated with the complexes may lead to direct hydrolysis of diester bonds by attacking the phosphorus, resulting in a trigonal bipyramidal phosphorus intermediate leading to cleavage of one of the phosphodiester bonds of DNA. It is also believed that intramolecular nucleophilic activation essential for hydrolytic cleavage may take place, due to the associated water molecules. Attempts were also made to study the dependence of cleavage on altering the incubation period by 30 min in which only a similar electrophoretic pattern is observed. The nuclease activity of complexes in the absence of any co-reactant is in the order **3** > **2** > **1**.

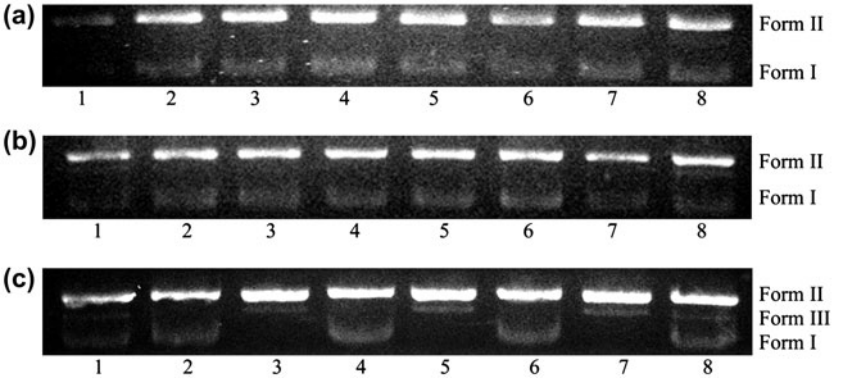

Figure 4. Agarose gel electrophoresis diagram (4a–c) showing the cleavage of pBR322 DNA by **1–3** in Tris–HCl/NaCl buffer (pH 7.2) and incubated for 90 min at 37 °C. Lane 1, DNA control; Lane 2, DNA + **1** (6.25 μM) or **2**/**3** (50 μM); Lane 3, DNA + **1** (6.25 μM) or **2**/**3** (50 μM) + H_2O_2; Lane 4, DNA + **1** (12.5 μM) or **2**/**3** (100 μM); Lane 5, DNA + **1** (12.5 μM) or **2**/**3** (100 μM) + H_2O_2; Lane 6, DNA + **1** (25 μM) or **2**/**3** (200 μM); Lane 7, DNA + **1** (25 μM) or **2**/**3** (200 μM) + H_2O_2; Lane 8, DNA + H_2O_2.

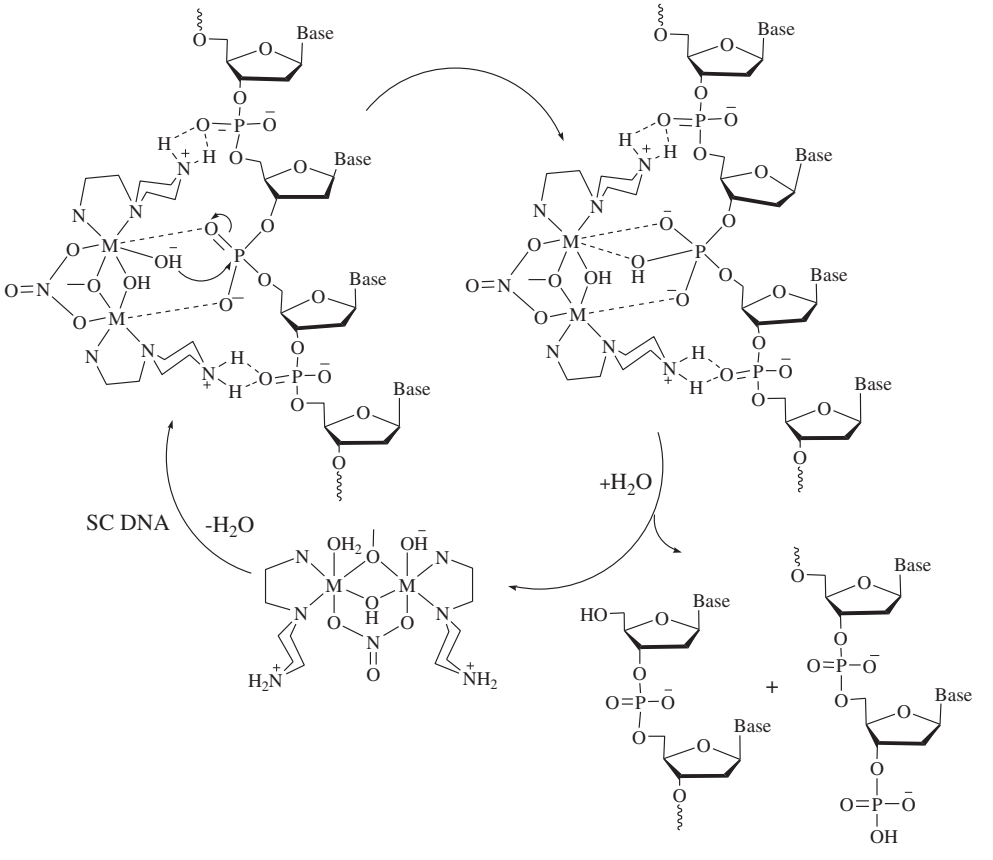

Scheme 2. A plausible mechanism for hydrolytic cleavage of DNA by **1–3**.

3.5.2. Nuclease activity in the presence of co-reactant. Oxidative cleavage is another form of nuclease activity which is usually carried out in the presence of a co-reactant. Lanes 3, 5, and 7 [figure 4(a)–(c)] represent the nuclease activity of the complexes in the presence of H_2O_2 as co-reactant. Interestingly for **3**, all three forms are visible on the gel, suggesting that **3** is involved in double-strand DNA cleavage to generate Form III (LC) before converting all of the Form I (SC) to Form II (NC) through single-strand breaking [figure 4(c)], showing prominent cleavage efficacy of **3** in the presence of co-reactant. In order to gain information on the involvement of reactive oxygen species (ROS), cleavage activity was carried out in the presence of the hydroxyl radical scavenger DMSO [50] for all complexes and inhibition of nuclease activity was observed, suggesting active participation of diffusible hydroxyl radical as ROS [19, 51]. A suitable pathway for generation of ROS necessary for nuclease activity is depicted in scheme S1 (Supplementary material). Under the experimental conditions, cleavage ability of complexes follows the order **3** > **2** > **1**, inferring that these complexes are good nuclease agents.

The nuclease activity of **1–3** appears to follow both hydrolytic and oxidative via free radical pathways similar to other reported phenoxo-bridged complexes [18, 52, 53]. The electrophoretic pattern also shows higher nuclease activity in the presence of the co-reactant H_2O_2.

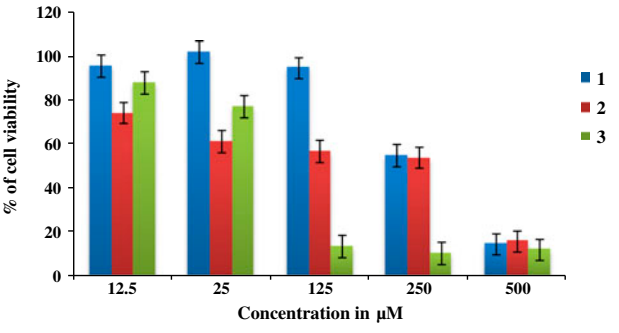

Figure 5. Concentration of **1–3** in µM *vs.* % of cell viability.

3.6. *Cytotoxic activity*

Cytotoxicities of **1–3** were examined on human epidermoid carcinoma cell lines (A431), by maintaining the cells in varying concentrations of the complexes for 24 h, using the MTT reduction assay. This assay is an index of cell viability by detecting the reduction of yellow tetrazolium salt to purple-blue formazan, developed as a result of a metabolic change which is a mitochondrial enzyme activity of succinate dehydrogenase in living cells. The inhibitory concentration required to reduce the size of cell population by 50% (IC_{50} value) for **1–3** are 305, 204, and 80 µM, respectively. Results of the MTT assay (figure 5) clearly indicate that these complexes inhibited the growth of epithelial cancer cells significantly in a dose-dependent manner. A considerable inhibitory effect is observed for **1** only beyond 125 µM concentrations. The cytotoxic activity of **2** is gradually increased with increasing concentration of complex from 12.5 µM onwards. Complex **3** exhibits more reduction in the viability of carcinoma cells than **1** and **2**, because its IC_{50} value is the least among the three complexes. Significant activity on cell lines is observed for **3** beyond 25 µM concentration and even at a minimal concentration of 125 µM itself, the cell viability was found to be as low as 13%.

The growth inhibition of carcinoma cells is due to inhibition of replication and transcription processes, which arises due to interaction of the metal complexes with DNA [54, 55]. Based on IC_{50} values, the cytotoxicity of the complexes can be expressed in the order **3** > **2** > **1** and the same trend is observed in the nuclease activity. These observations suggest prominent cytotoxicity of the complexes is consistent with the nuclease activity. The significant cytotoxicity of **3** is comparable to that observed for other dinuclear Cu(II) complexes tested against human heptocellular carcinoma cell line SMMC–7721 and human lung adenocarcinoma cell line A549 [56].

4. Conclusion

The present contribution describes the synthesis of a series of homo dinuclear cobalt(II), nickel(II), and copper(II) complexes (**1–3**) using an "end-off" compartmental ligand, HL. The structure of **1** was established by X-ray crystallography. X-ray crystal structural investigation of **1** along with spectral studies revealed distorted octahedral geometry around the metal ions. The temperature-dependent magnetic properties of **3** show a strong antiferromagnetic interaction between paramagnetic centers. The dinuclear copper(II) complex **3**

represents significant cytotoxic and nuclease activities. On the whole, a similar trend is observed for chemical nuclease and cytotoxic activities of the complexes, which follow the order **3** > **2** > **1**. Detailed antitumor mechanistic investigations on the dinuclear phenoxo-bridged "end-off" copper(II) complex and other complexes with related ligands bearing different substituents on the aromatic ring are currently underway.

Supplementary material

CCDC 880739 contains the supplementary crystallographic data for the dinuclear Co(II) complex **1**. These data can be obtained free of charge via http://www.ccdc.cam.ac.uk/conts/retrieving.html (or from the Cambridge Crystallographic Data Center, 12 Union Road, Cambridge CB2 1EZ, UK; Fax: +44 1223 336 0330).

Acknowledgements

AKR gratefully acknowledges the financial assistance from the University Grants Commission (UGC), New Delhi, through the Major Research Project grant [F. No. 39-797/2010 SR)]. CK thanks UGC, New Delhi, for providing financial assistance in the form of fellowship. The authors thank Dr Sultan Ahamed Ismail, DSc, Head, Department of Biotechnology, The New College (Autonomous), for providing facilities to carry out the chemical nuclease activity.

References

[1] B. Rosenberg, L. Vancamp, J.E. Trosko, V.H. Mansour. *Nature*, **222**, 385 (1969).
[2] A.M.J. Fichtinger-Schepman, J.L. Van der veer, J.H.J. Den Hartog, P.H.M. Lohman, J. Reedijk. *Biochemistry*, **24**, 707 (1985).
[3] S.J. Lippard, J.M. Berg. *Principles of Bioinorganic Chemistry*, University Science Books, Mill Valley, CA (1994).
[4] P.J. Dyson, G. Sava. *Dalton Trans.*, 1929 (2006).
[5] P.A. Vigato, S. Tamburini. *Coord. Chem. Rev.*, **252**, 1871 (2008).
[6] G. Ambrosi, M. Formica, V. Fusi, L. Giorgi, M. Micheloni. *Coord. Chem. Rev.*, **252**, 1121 (2008).
[7] A. Greatti, M.A. de Brito, A.J. Bortoluzzi, A.S. Ceccato. *J. Mol. Struct.*, **688**, 185 (2004).
[8] I.A. Koval, D. Pursche, A.F. Stassen, P. Gamez, B. Krebs, J. Reedijk. *Eur. J. Inorg. Chem.*, **2003**, 1669 (2003).
[9] P. Nordlund, B.M. Sjöberg, H. Eklund. *Nature*, **345**, 593 (1990).
[10] M.A. Holmes, I. Le Trong, S. Turley, L.C. Sieker, R.E. Stenkamp. *J. Mol. Biol.*, **218**, 583 (1991).
[11] F. Rahaman, O.B. Ijare, Y. Jadegoud, B.H.M. Mruthyunjayaswamy. *J. Coord. Chem.*, **62**, 1457 (2009).
[12] N.A. Illán-Cabeza, F. Hueso-Ureña, M.N. Moreno-Carretero, J.M. Martínez-Martos, M.J. Ramírez-Expósito. *J. Inorg. Biochem.*, **102**, 647 (2008).
[13] R.N. Patel, N. Singh, K.K. Shukla, U.K. Chauhan, S. Chakraborty, J. Niclós-Gutiérrez, A. Castiñeiras. *J. Inorg. Biochem.*, **98**, 231 (2004).
[14] P.A. Vigato, V. Peruzzo, S. Tamburini. *Coord. Chem. Rev.*, **256**, 953 (2012).
[15] T. Koga, H. Furutachi, T. Nakamura, N. Fukita, M. Ohba, K. Takahashi, H. Ōkawa. *Inorg. Chem.*, **37**, 989 (1998).
[16] M. Suzuki, H. Furutachi, H. Ōkawa. *Coord. Chem. Rev.*, **200–202**, 105 (2000).
[17] K.S. Banu, T. Chattopadhyay, A. Banerjee, S. Bhattacharya, E. Suresh, M. Nethaji, E. Zangrando, D. Das. *Inorg. Chem.*, **47**, 3121 (2008).
[18] T. Chattopadhyay, M. Mukherjee, A. Mondal, P. Maiti, A. Banerjee, K.S. Banu, S. Bhattacharya, B. Roy, D.J. Chattopadhyay, T.K. Mondal, M. Nethaji, E. Zangrando, D. Das. *Inorg. Chem.*, **49**, 3121 (2010).
[19] T.A. Yousef, G.M. Abu El-Reash, O.A. El-Gammal, R.A. Bedier. *J. Mol. Struct.*, **1029**, 149 (2012).
[20] L.F. Lindoy, G.V. Meehan, N. Svenstrup. *Synthesis*, 1029 (1998).

[21] C.N. Verani, E. Rentschler, T. Weyhermüller, E. Bill, P. Chaudhuri. *J. Chem. Soc., Dalton Trans.*, 251 (2000).
[22] W.L.E. Armarego, D.D. Perrin. *Purification of Laboratory Chemicals*, 4th Edn, Butterworth-Heinemann, Wodburn, MA (2000).
[23] Bruker-Nonius. *APEX-II and SAINT-plus (Version 7.06a)*, Bruker AXS, Inc., Madison, WI (2004).
[24] *SADABS*, Bruker AXS, Inc., Madison, WI (2001).
[25] A. Altomare, G. Cascarano, C. Giacovazzo, A. Guagliardi. *J. Appl. Crystallogr.*, **26**, 343 (1993).
[26] T. Mosmann. *J. Immunol. Methods*, **65**, 55 (1983).
[27] H. Adams, S. Clunas, D.E. Fenton, G. Handley, P.E. McHugh. *Inorg. Chem. Commun.*, **5**, 1044 (2002).
[28] D. Saravanakumar, N. Sengottuvelan, G. Priyadarshni, M. Kandaswamy, H. Okawa. *Polyhedron*, **23**, 665 (2004).
[29] M. Vicente, C. Lodeiro, H. Adams, R. Bastida, A.D. Blas, D.E. Fenton, A. Macías, A. Rodríguez, T.R. Rodríguez-Blas. *Eur. J. Inorg. Chem.*, **2000**, 1015 (2000).
[30] G.S. Patterson, R.W. Holm. *Bioinorg. Chem.*, **4**, 257 (1975).
[31] A.B.P. Lever. *Inorganic Electronic Spectroscopy*, Elsevier, Amsterdam (1984).
[32] V.B. Rana, P. Singh, D.P. Singh, M.P. Teotia. *Polyhedron*, **1**, 377 (1982).
[33] M. Thirumavalavan, P. Akilan, M. Kandaswamy, K. Chinnakali, G.S. Kumar, H.K. Fun. *Inorg. Chem.*, **42**, 3308 (2003).
[34] R.C. Aggarwal, N.K. Singh, R.P. Singh. *Inorg. Chem.*, **20**, 2794 (1981).
[35] A.A. Nejo, G.A. Kolawole, A.O. Nejo. *J. Coord. Chem.*, **63**, 4398 (2010).
[36] K.R. Krishnapriya, M. Kandaswamy. *Polyhedron*, **24**, 113 (2005).
[37] Md.J. Hossain, M. Yamasaki, M. Mikuriya, A. Kuribayashi, H. Sakiyama. *Inorg. Chem.*, **41**, 4058 (2002).
[38] B. Roopashree, V. Gayathri, H. Mukund. *J. Coord. Chem.*, **65**, 1354 (2012).
[39] B. Bleaney, K.D. Bowers. *Proc. R. Soc. London, Ser. A*, **214**, 451 (1952).
[40] L.K. Thompson, S.K. Mandal, S.S. Tandon, J.N. Bridson, M.K. Park. *Inorg. Chem.*, **35**, 3117 (1996).
[41] K. Bertoncello, G.D. Fallon, J.H. Hodgkin, K.S. Murray. *Inorg. Chem.*, **27**, 4750 (1988).
[42] K. Shanmuga Bharathi, S. Sreedaran, A. Kalilur Rahiman, K. Rajesh, V. Narayanan. *Polyhedron*, **26**, 3993 (2007).
[43] S. Mukherjee, T. Weyhermüller, E. Bothe, K. Wieghardt, P. Chaudhuri. *Eur. J. Inorg. Chem.*, **2003**, 863 (2003).
[44] S.S. Massoud, F.R. Louka, W. Xu, R.S. Perkins, R. Vicente, J.H. Albering, F.A. Mautner. *Eur. J. Inorg. Chem.*, **2011**, 3469 (2011).
[45] A.S. Sitlani, E.C. Long, A.M. Pyle, J.K. Barton. *J. Am. Chem. Soc.*, **114**, 2303 (1992).
[46] N. Raman, K. Pothiraj, T. Baskaran. *J. Mol. Struct.*, **1000**, 135 (2011).
[47] Q.L. Zhang, J.G. Liu, H. Chao, G.Q. Xue, L.N. Ji. *J. Inorg. Biochem.*, **83**, 49 (2001).
[48] J. Qian, W. Gu, H. Liu, F. Gao, L. Feng, S. Yan, D. Liao, P. Cheng. *Dalton Trans.*, 1060 (2007).
[49] N.A. Rey, A. Neves, P.P. Silva, F.C.S. Paula, J.N. Silveira, F.V. Botelho, L.Q. Vieira, C.T. Pich, H. Terenzi, E.C. Pereira-Maia. *J. Inorg. Biochem.*, **103**, 1323 (2009).
[50] J.A. Cowan. *Curr. Opin. Chem. Biol.*, **5**, 634 (2001).
[51] Y.Y. Kou, J.L. Tian, D.D. Li, H. Liu, W. Gu, S.P. Yan. *J. Coord. Chem.*, **62**, 2182 (2009).
[52] P.R. Reddy, A. Shilpa, N. Raju, P. Raghavaiah. *J. Inorg. Biochem.*, **105**, 1603 (2011).
[53] Q.R. Cheng, J.Z. Chen, H. Zhou, Z.Q. Pan. *J. Coord. Chem.*, **64**, 1139 (2011).
[54] S. Ramakrishnan, E. Suresh, A. Riyasdeen, M.A. Akbarsha, M. Palaniandavar. *Dalton Trans.*, 3245 (2011).
[55] S. Carotti, A. Guerri, T. Mazzei, L. Messori, E. Mini, P. Orioli. *Inorg. Chim. Acta*, **281**, 90 (1998).
[56] X.L. Wang, M. Jiang, Y.T. Li, Z.Y. Wu, C.W. Yan. *J. Coord. Chem.*, **66**, 1985 (2013).